Pergamon International Journal of Machine Tools & Manufacture 41 (2001) 2213–2231

INTERNATIONAL JOURNAL OF MACHINE TOOLS & MANUFACTURE DESIGN, RESEARCH AND APPLICATION

Mechanics and dynamics of general milling cutters. Part II: inserted cutters

S. Engin [1], Y. Altintas [*]

The University of British Columbia, Department of Mechanical Engineering, Vancouver, British Columbia, Canada V6T 1Z4

Received 9 February 2001; accepted 2 April 2001

Abstract

Inserted cutters are widely used in roughing and finishing of parts. The insert geometry and distribution of inserts on the cutter body vary significantly in industry depending on the application. This paper presents a generalized mathematical model of inserted cutters for the purpose of predicting cutting forces, vibrations, dimensional surface finish and stability lobes in milling. In this paper, the edge geometry is defined in the local coordinate system of each insert, and placed and oriented on the cutter body using the cutter's global coordinate system. The cutting edge locations are defined mathematically, and used in predicting the chip thickness distribution along the cutting zone. Each insert may have a different geometry, such as rectangular, convex triangular or a mathematically definable edge. Each insert can be placed on the cutter body mathematically by providing the coordinates of the insert center with respect to the cutter body center. The inserts can be oriented by rotating them around the cutter body, thus each insert may be assigned to have different lead and axial rake angles. By solving the mechanics and dynamics of cutting at each edge point, and integrating them over the contact zone, it is shown that the milling process can be predicted for any inserted cutter. A sample of inserted cutter modeling and analysis examples are provided with experimental verifications.

Keywords: Inserted cutters; Cutting forces; Chatter vibrations

1. Introduction

Inserted face and end milling cutters are widely used in industry. Face milling cutters have evenly or unevenly spaced inserts, and are used in removing excess material from the face of

* Corresponding author. Tel.: +1-604-822-5622; fax: +1-604-822-2403.
E-mail address: altintas@mech.ubc.ca (Y. Altintas).
[1] Currently with Pratt and Whitney Canada, 1000 Marie-Victorin, Longueuil, Quebec, Canada J4G 1A1.

0890-6955/01/$ - see front matter
PII: S0890-6955(01)00046-3

Nomenclature

a, b rectangular insert width and height
dF_t, dF_r, dF_a differential tangential, radial and axial force components acting on a chip element, respectively
F_x, F_y, F_z cutting forces in X, Y and Z directions, respectively
$h(\phi, z)$ instantaneous chip thickness
I_r, I_z insert center radial and axial distance from cutter tip, respectively
K_{tc}, K_{rc}, K_{ac} cutting force coefficients in tangential, radial and axial directions, respectively
K_{te}, K_{re}, K_{ae} cutting coefficients in tangential, radial and axial directions, respectively
O, O' cutter and insert center points
R, θ_s, θ_e, o_f convex triangular insert dimensions
$\boldsymbol{R}_x(\beta)$, $\boldsymbol{R}_y(\delta)$, $\boldsymbol{R}_z(\phi)$ insert rotation matrices for X, Y and Z, respectively
$\underline{\boldsymbol{T}}_M$ total transformation matrix for the insert
$\underline{\boldsymbol{V}}_{CE}$ cutting edge position vector from insert center
$\underline{\boldsymbol{V}}_{CER}$ cutting edge position vector from insert center after rotations
$\underline{\boldsymbol{V}}_{IC}$ insert center position vector from cutter center
$\boldsymbol{V}_p$ cutting edge position vector from cutter center
u, v, w insert local coordinate system
X, Y, Z cutter coordinate system
β, δ, ϕ insert rotation angles around X, Y and Z axes, respectively

parts such as transmission boxes, engine blocks or machine tool columns and beds. Inserts are distributed in both radial and axial directions on indexed end mills. Indexed cutters are used in removing massive amounts of material from the periphery of parts such as aircraft spars and airframe support structures, and for rough pocketing of dies and molds. The distribution of inserts may be regular or arbitrary depending on the application. In order to improve the surface finish, chatter stability and cutting force balancing on the cutter body, inserts with various shapes can be placed on the milling cutter body.

The industry requires a generalized mathematical model which allows the analysis of all inserted milling cutters used in practice [1]. However, research in the past has mainly focused on modeling of the mechanics and dynamics of special cutter geometries. Fu et al. [2] provided a comprehensive model of inserted face milling cutters. They modeled rectangular inserts with corner radius, and introduced equivalent lead and rake angles, which are related to experimentally identified cutting coefficients. Fu et al.'s work [2] became a basis for a number of successive mechanistic models in milling, and led to the improved static and dynamic modeling of milling [3]. The mechanistic approach allowed the integration of milling mechanics and the optimization of cutting conditions during tool path planning on CAD/CAM systems [4,5]. The cutting forces are assumed to be proportional to the instantaneous chip area in most face milling cases, but the variation of cutting pressure along the curved cutting edge is also considered in some of the more rigorous models [6]. Spiewak [7] presented an analytical method in integrating the spindle tilt,

runout and eccentricity in identifying the chip thickness. However, a generalized handling of the mechanics and dynamics of inserted end mills has not received similar attention. The majority of research up until now has focused on the accurate identification of chip load in static and dynamic milling, and identification of cutting coefficients for a single insert.

This paper presents a generalized model of the cutting force system in inserted cutters. The cutting edge is defined mathematically in a local coordinate system of each insert. Each insert may have a different geometry, such as rectangular, convex triangular or a mathematically definable edge. Each insert can be placed on the cutter body mathematically by providing the coordinates of the insert center with respect to the cutter body center. The inserts can be oriented by rotating them around the cutter body, thus each insert may be assigned to have different lead and axial rake angles. The cutting edge geometry of each insert on the cutter is mathematically expressed. The cutter is divided into small disk elements, and the mechanics and dynamics of milling can be solved for each cutting edge element. The literature provides various approaches for determining the cutting coefficient and dynamic chip load as a function of local cutting edge geometry. The reported process modeling techniques, which are not repeated but only cited here, are used along the cutting edge. By integrating the structural dynamics of workpiece and cutter into the mathematical model, the performance of a general indexed cutter can be simulated. The generalized model allows prediction of cutting forces, dimensional surface finish, chatter and forced vibrations, and chatter stability lobes for a variety of inserted face and helical end mills. The paper provides milling examples for two different inserted end mills.

Henceforth, the paper is organized as follows. The geometric modeling of inserted cutters is provided in Section 2. The mechanics and dynamics of milling used in this particular work are summarized in Section 3, and the details of the process models are cited to the relevant literature. Prediction of cutting forces, vibrations, dimensional surface finish and chatter stability was demonstrated using two different inserted helical end mils. The simulation and experimental results are given in Section 4, and the paper is concluded with the summary of contributions in Section 5.

2. Generalized geometric model of inserted cutters

The purpose of the geometric model is to predict the mechanics and dynamics of cutters with arbitrary insert shapes and distribution. First, the mathematical model of one insert placed on a cutter body is given and then the definition of a general cutter with varying inserts along its periphery is presented.

2.1. Mathematical model of insert

The cutter body is defined in the Cartesian coordinate system (X, Y, Z), and the center of the insert is aligned with a second coordinate system (u, v, w), see Fig. 1. A vector between the cutter tip and insert centers is

$$\vec{\boldsymbol{V}}_{\mathrm{IC}} = -\sin\phi I_r \vec{\boldsymbol{i}} + \cos\phi I_r \vec{\boldsymbol{j}} + I_z \vec{\boldsymbol{k}}, \tag{1}$$

where I_r is the radial offset in the XY plane and I_z is the axial offset of the insert center from the

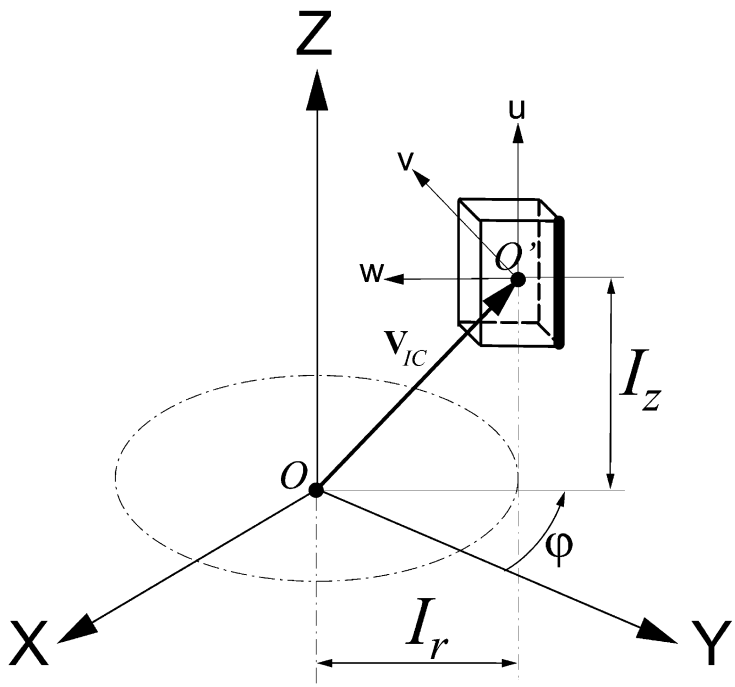

Fig. 1. Location vector of insert center on the cutter.

cutter axis (Fig. 1). The face of the insert where the cutting edge lies is aligned with the *uw* plane of the insert coordinate system (i.e., v=0). The insert center is indexed by an angular distance of ϕ measured counterclockwise from the Y axis, see Fig. 1. The insert is placed on the cutter body using the vector defined in Eq. (1).

The insert shapes can vary depending on the application and manufacturer. Two of the most common insert shapes are considered to illustrate the generalized modeling approach, see Fig. 2.

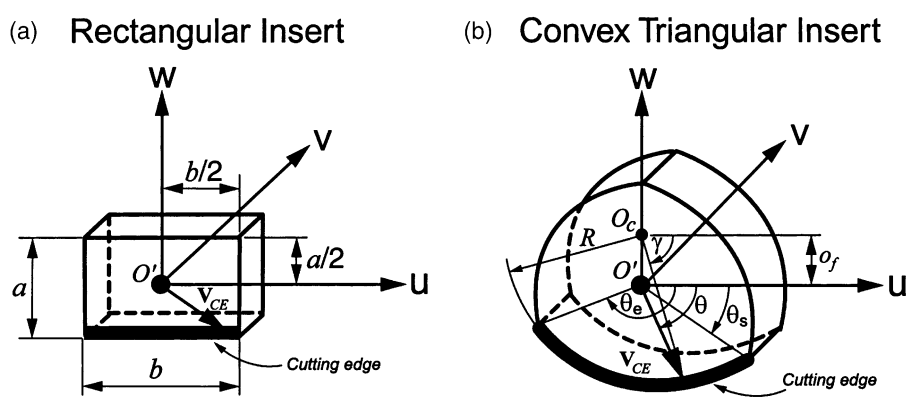

Fig. 2. Geometry of inserts.

The rectangular insert is defined by the cutting edge length (b) and insert width (a). The convex triangular insert is defined by the radius (R) of the curved cutting edge, the offset (o_f) between the insert center (O') and the cutting edge curvature center (O_c), and by the angular boundaries (θ_s, θ_e) of the cutting edge measured on the uw plane in clockwise direction from the local axis (u). The points along the cutting edge of the insert are defined by the vector $\vec{V}_{CE}$ in coordinate system (u, v, w),

$$\vec{V}_{CE}=u\vec{i}+v\vec{j}+w\vec{k}, \tag{2}$$

where

$$-\frac{b}{2}\le u\le\frac{b}{2};\quad v=0;\quad w=\frac{a}{2} \qquad \text{for a rectangular insert}$$

$$\left.\begin{aligned} &u=R\cos\gamma;\quad v=0;\quad w=-R\cos\gamma+o_f\\ &\gamma=\theta+\sin^{-1}\left(\frac{o_f}{R}\cos\theta\right)\ \text{for}\ \theta_s\le\theta\le\theta_e \end{aligned}\right\} \qquad \text{for a convex triangular insert}$$

Note that uvw plane of the insert's coordinate system is aligned with the insert face, which contains the cutting edge (i.e., $v=0$). The insert's cutting edge is defined locally in the insert coordinate system (u, v, w).

Each insert can be oriented on the cutter body by rotating it around the global cutter body axes X, Y and Z (Fig. 3). The insert rotation is defined by *lead angle* (δ) around the Y axis, *axial rake angle* (β) around the X axis, and *index angle* (ϕ) around the Z axis. The corresponding rotation matrices for X, Y and Z are respectively as follows

$$\boldsymbol{R}_y(\beta)=\begin{bmatrix}1 & 0 & 0\\ 0 & \cos\beta & \sin\beta\\ 0 & -\sin\beta & \cos\beta\end{bmatrix};\quad \boldsymbol{R}_y(\delta)=\begin{bmatrix}\sin\delta & 0 & -\cos\delta\\ 0 & 1 & 0\\ \cos\delta & 0 & \sin\delta\end{bmatrix};\quad \boldsymbol{R}_z(\phi)=\begin{bmatrix}-\sin\phi & -\cos\phi & 0\\ \cos\phi & -\sin\phi & 0\\ 0 & 0 & 1\end{bmatrix}. \tag{3}$$

If the insert is rotated about all three axes, the resulting transformation matrix is

$$\boldsymbol{T}_M=\boldsymbol{R}_z(\phi)\cdot\boldsymbol{R}_x(\beta)\cdot\boldsymbol{R}_y(\delta) \tag{4}$$

$$=\begin{bmatrix}-\sin\phi\sin\delta-\cos\phi\sin\beta\cos\delta & -\cos\phi\cos\beta & \sin\phi\cos\delta-\cos\phi\sin\beta\sin\delta\\ \cos\phi\sin\delta-\sin\phi\sin\beta\cos\delta & -\sin\phi\cos\beta & -\cos\phi\cos\delta-\sin\phi\sin\beta\sin\delta\\ \cos\beta\cos\delta & -\sin\beta & \cos\beta\sin\delta\end{bmatrix}.$$

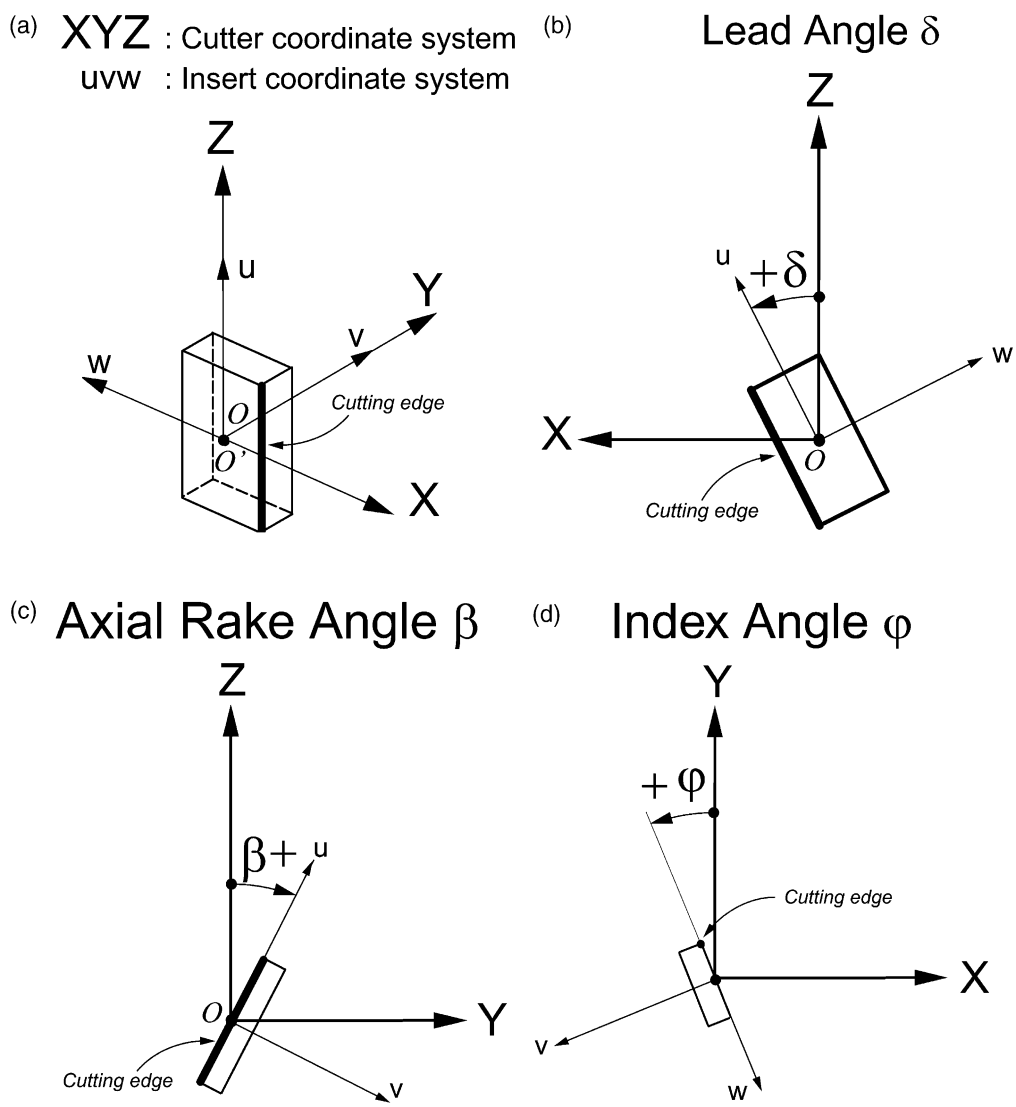

Fig. 3. The insert rotations. (a) Cutter (XYZ) and insert (UVW) coordinates; (b) rotation about Y axis with δ lead angle; (c) rotation about X axis with β axial rate angle; and (d) rotation about Z axis with ϕ index angle.

The coordinates of the cutting edge in the insert coordinate system become (Fig. 4)

$$\boldsymbol{V}_{\mathrm{CER}}=\boldsymbol{T}_{\mathrm{M}}\cdot\boldsymbol{V}_{\mathrm{CE}}=[\boldsymbol{T}_{\mathrm{M}}]\begin{bmatrix}u\\v\\w\end{bmatrix}. \tag{5}$$

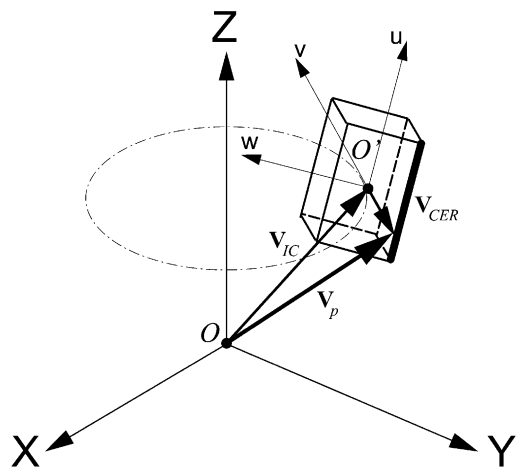

Fig. 4. The cutting edge position vector.

The final position of the cutting edge with respect to the cutter body coordinate system becomes

$$\vec{\boldsymbol{V}}_{\mathrm{p}}=\vec{\boldsymbol{V}}_{\mathrm{IC}}+\vec{\boldsymbol{V}}_{\mathrm{CER}}=-\sin\phi I_r\vec{\boldsymbol{i}}+\cos\phi I_r\,\vec{\boldsymbol{j}}+I_z\vec{\boldsymbol{k}}+[\boldsymbol{T}_{\mathrm{m}}]\begin{bmatrix}u\\v\\w\end{bmatrix}=[-\sin\phi(u\sin\delta-w\cos\delta+I_r)$$

$$-\cos\phi\sin\beta(u\cos\delta+w\sin\delta)-v\cos\phi\cos\beta]\vec{\boldsymbol{i}}+[\cos\phi(u\sin\delta-w\cos\delta+I_r) \tag{6}$$

$$-\sin\phi\sin\beta(u\cos\delta+w\sin\delta)-v\sin\phi\cos\beta]\vec{\boldsymbol{j}}+[\cos\beta(u\cos\delta+w\sin\delta)-v\sin\beta$$

$$+I_z]\vec{\boldsymbol{k}}.$$

Once the insert center location (I_r, I_z), orientation on the cutter body (δ, β, ϕ) and edge dimensions (a, b; R, θ_s, θ_e) are specified, a point on the cutting edge can be evaluated for a given elevation or axial depth of cut position (z) from Eq. (6).

2.2. Mathematical model of multiple inserts

There are various inserted cutters used in industry depending on machining applications. There may be identical inserts placed on the periphery of the cutter with equal pitch spacing (i.e., face milling cutters), helical flutes where each flute may contain multiple inserts, or randomly distributed inserts with different shapes and at different locations both in radial and axial directions. A generalized cutter design matrix ($\boldsymbol{D}_{\mathrm{M}(6\times N)}$) is used in defining a cutter with a general insert distribution

$$D_M = \begin{bmatrix} t_{11} & t_{12} & t_{13} & \ldots; & t_{21} & t_{22} & \ldots; & \ldots \\ I_{z11} & I_{z12} & I_{z13} & \ldots; & I_{z21} & I_{z22} & \ldots; & \ldots \\ I_{r11} & I_{r12} & I_{r13} & \ldots; & I_{r21} & I_{r22} & \ldots; & \ldots \\ \delta_{11} & \delta_{12} & \delta_{13} & \ldots; & \delta_{21} & \delta_{22} & \ldots; & \ldots \\ \beta_{11} & \beta_{12} & \beta_{13} & \ldots; & \beta_{21} & \beta_{22} & \ldots; & \ldots \\ \underbrace{\varphi_{11}}_{1.insert} & \underbrace{\varphi_{12}}_{2.insert} & \underbrace{\varphi_{13}}_{3.insert} & \underbrace{\ldots;}_{\ldots} & \underbrace{\varphi_{21}}_{1.insert} & \underbrace{\varphi_{22}}_{2.insert} & \underbrace{\ldots;}_{\ldots} & \underbrace{\ldots}_{\ldots} \\ \multicolumn{4}{c}{\underbrace{\qquad\qquad}_{1.flute}} & \multicolumn{3}{c}{\underbrace{\qquad\qquad}_{2.flute}} & \end{bmatrix} \tag{7}$$

where N is the number of inserts on the cutter. The first and second digits of subindices represent flute number and insert order number from the tool tip, respectively. Note that it is not necessary to have equal numbers of inserts on each flute. Each column represents one insert with its type and position on the cutter body. The first element (t) of each column represents the insert type — i.e., t=0: no insert; t=1…10: rectangular insert family; t=11…20 triangular insert family. The remaining five parameters define the position and orientation of the insert on the cutter body. Rectangular inserts have two parameters that are width (a) and length (b) [Fig. 2(a)]. The convex triangular insert has four parameters that are the starting angle (θ_s) and the end angle (θ_e), the radius of arc (R) and the arc radius center offset from the insert center (o_f) [Fig. 2(b)]. Each insert shape is stored separately in a database with its associated dimensions. The generalized cutter design matrix has been used in the calculations and database.

3. Modeling of cutting forces

Consider that differential cutting forces (dF_t, dF_r, dF_a) are produced when cutting an infinitesimal chip element which has a local uncut chip thickness of $h(\phi, z)$ normal to the cutting edge, chip height of dz and curved edge contact length of dS (Fig. 5)

$$\left.\begin{aligned} dF_t &= K_{te}(z)\, dS + K_{tc}(z) h(\phi, z)\, dz \\ dF_r &= K_{re}(z)\, dS + K_{rc}(z) h(\phi, z)\, dz \\ dF_a &= K_{ae}(z)\, dS + K_{ac}(z) h(\phi, z)\, dz \end{aligned}\right\} \tag{8}$$

The edge force cutting coefficients K_{te}, K_{re} and K_{ae} represent the non-shearing flank line contact forces, and the force coefficients K_{tc}, K_{rc} and K_{ac} represent shear or rake face contact pressure. The linearized force model used in Eq. (8) is presented in detail by Budak et al. [8]. It should be noted that the inserts used in industry might have varying rake face and curvature along their

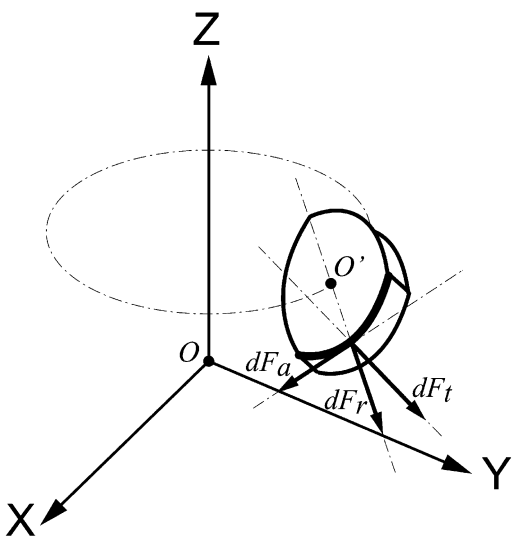

Fig. 5. Three-dimensional cutting edge profile on the insert and cutting force directions.

cutting edge. For example, chip breaking grooves and non-uniform rake face may exist on each insert. The cutting coefficients can be identified from orthogonal cutting parameters (average shear stress, shear angle and friction coefficient) by transforming them into the oblique cutting domain [8], if the rake face is uniform like in regular end mills. However, if the insert's cutting edge has a chamfer or radius, and the rake face of the insert is non-uniform, orthogonal to oblique cutting transformation may not lead to an accurate evaluation of cutting coefficients [6]. Depending on the insert shape and cutting edge geometry, it may be more appropriate to use mechanistic models in identifying the cutting coefficients as a function of edge position (z), cutting speed and local chip thickness. The mechanistic approaches for the identification of cutting coefficients are presented in the literature [2–4,6]. The evaluation of chip thickness with and without chatter vibrations has been presented in detail by Altintas and Lee [9]. Details of the mechanistic identification of cutting coefficients and milling process modeling can be found in the cited literature, and are used but not repeated here [10]. The cutter is divided into small axial disk elements with a differential height of dz. The uncut chip thickness removed by each differential segment along the insert is identified by considering the trochoidal motion of the milling [11] and the regenerative chatter vibration of both cutter and workpiece [12]. If the insert has roundness, the chip thinning is considered using a similar method as in ball end milling [9]. The differential cutting forces are evaluated and transformed into Cartesian coordinates of the cutter similar to the method used for helical end mills, see Part I of the paper [13]. The differential forces are summed along all inserts, which are in contact with the workpiece. The resulting cutting forces in the three directions are applied to the structural dynamic models of cutter and workpiece to evaluate the structural displacements and their influence on the regenerative chip thickness. The dynamic chip thickness [$h(\phi, z)$] is evaluated at small time intervals by rotating the cutter and feeding the workpiece. The time-domain simulation model allows predictions of dynamic chip thickness, cutting forces, vibrations of both cutter and workpiece along the depth of cut, surface finish and chatter stability lobes [9,14]. The chatter stability lobes for the inserted cutters are also identified in the frequency

domain using the analytical solution proposed by Altintas and Budak [15]. The cited models of milling process mechanics, kinematics, dynamics and process simulations are all used here, and the readers are referred to the indicated publications for a comprehensive understanding of the models.

4. Simulation and experimental results

The proposed generalized inserted cutter model, and its corresponding mechanics and dynamics, are integrated into the comprehensive milling process simulation package [16]. The advanced simulation program contains all the process models cited in the previous section. Two sample cases are presented here to illustrate the proposed model.

4.1. Milling of Al7075 with Cutter I

A two-fluted helical inserted cutter with 25.4 mm diameter and four rectangular inserts on each flute is modeled (Fig. 6). The cutter body is Mitsubishi BAP300R 1608WL16, with Mitsubishi

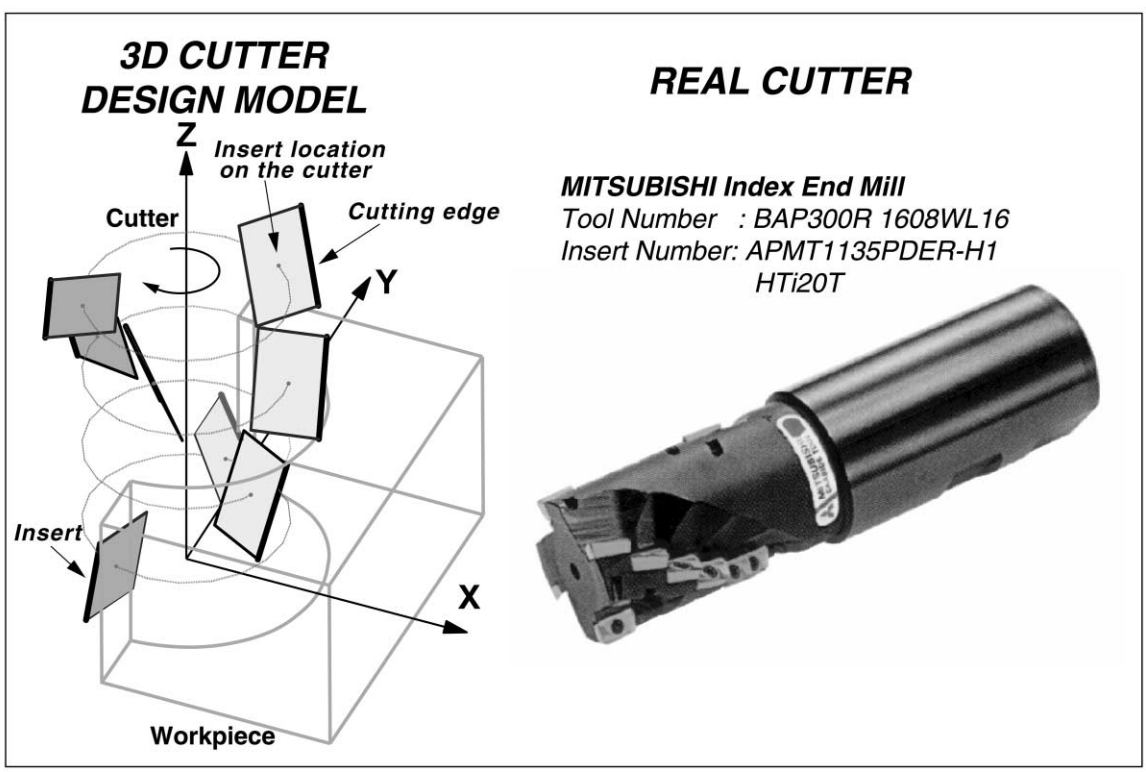

Fig. 6. Mitsubishi inserted cutter Cutter I (cutter number: BAP300R 1608WL16; insert number: APMT1135PDER-H1, "insert dimensions a=6.35 mm, b=9.8 mm", HTi20T). See Eq. (9) for insert location parameters. Shank diameter=25.4 mm, cutter diameter=25.4 mm, two flutes, four inserts on every flute.

APMT1135PDER-H1 HTi20T rectangular inserts (a=6.35 mm, b=9.8 mm). The design matrix of the cutter is constructed as

$$\boldsymbol{D}_{\mathrm{M}}=\begin{bmatrix} 2 & 2 & 2 & 2 & ; & 2 & 2 & 2 & 2 \\ 4.6 & 13.1 & 17.7 & 22.3 & ; & 4.7 & 13.2 & 17.8 & 22.4 \\ 9.5 & 9.5 & 9.5 & 9.5 & ; & 9.5 & 9.5 & 9.5 & 9.5 \\ 0.0 & 0.0 & 0.0 & 0.0 & ; & 0.0 & 0.0 & 0.0 & 0.0 \\ 20.0 & 20.0 & 20.0 & 20.0 & ; & 10.0 & 20.0 & 20.0 & 20.0 \\ 0.0 & 40.0 & 80.0 & 120.0 & ; & 190.0 & 270.0 & 310.0 & 350.0 \end{bmatrix}. \tag{9}$$

Note that the first insert of the second flute (row 5, column 5) has an axial rake of 10°, where the rest of the inserts have an axial rake of 20°. The lead angles of all inserts are zero (row 4). The cutter is used to machine Al7075. The cutting coefficients are identified mechanistically from the measured average cutting forces per tooth period. Slot milling tests were conducted with one insert by increasing the axial depth of cut with 1.0 mm increments up to the insert's edge length [8]. The insert's rake face geometry varies significantly along the cutting edge. Therefore the cutting coefficients are highly dependent on the axial location of the cutting edge point. The cutting coefficients are identified for each 1.0 mm segment. When the depth of cut is 5.0 mm for example, the measured average forces for 4.0 mm axial depth of cut were subtracted before identifying the cutting coefficients for the 5.0 mm edge zone. The cutting tests were conducted at a feed rate range of 0.025 to 0.200 mm/tooth at 0.025 mm/tooth increments. After identifying the cutting coefficients for each edge position, a satisfactory polynomial was fitted to represent them along the insert's cutting edge. The cutting coefficients identified for the two different inserts are given in Table 1. A statistical analysis result, the correlation coefficient, is provided for each set. The closeness of the correlation coefficient to unity represents the improved accuracy of the

Table 1
The cutting coefficients for Al7075 with Cutter I ($0 \le z \le 9.8$ mm). The edge contact position (z) is expressed in millimeters

Cutting coefficient	10° helix angle		20° helix angle	
	Fitted curve	Correlation coefficient	Fitted curve	Correlation coefficient
K_{tc} (N/mm^2)	$7.9z^2-90.4z+1073.5$	0.7984	$-5.6z^2+22.76z+925.4$	0.9003
K_{rc} (N/mm^2)	$25.98z^2-222.3z+795.1$	0.9198	$-13.0z^2+85.6z+409.1$	0.9242
K_{ac} (N/mm^2)	$19.55z^2-159.4z+294.55$	0.9164	$-15.3z^2+181.9z-227.6$	0.8241
K_{te} (N/mm)	$-0.34z^2-1.914z+38.78$	0.7796	$-0.04z^2-2.04z+33.86$	0.8006
K_{re} (N/mm)	$-3.15z^2+22.98z+23.80$	0.8071	$-0.46z^2+1.38z+53.86$	0.9672
K_{ae} (N/mm)	$-2.66z^2+27.56z-54.80$	0.9195	$-0.25z^2+2.56z-6.92$	0.7754

curve fitting. Higher-order polynomials were also used, but the improved accuracy was not sufficient to justify the complexity in expressing the cutting coefficients. The cutter is attached to a taper 40 spindle with a mechanical chuck. The transfer functions ($[\Phi_{xx}(s)]=\{x\}/\{F_x\}$, $[\Phi_{yy}(s)]=\{y\}/\{F_y\}$) of the cutter mounted on the spindle were measured with impact hammer tests, and the modal parameters identified are given in Table 2. The transfer function model has the following structure:

$$\frac{x}{F}=[\Phi_{xx}(s)]=\sum_{k=1}^{K}\frac{[R_{1x}+R_{2x}s]_k}{s^2+2\zeta_{x,k}\omega_{x,k}s+\omega_{x,k}^2},$$

where x and F are the vibration and force in the feed direction, respectively. $\zeta_{x,k}$ and $\omega_{x,k}$ are the damping ratio and natural frequency for mode k, and K is the number of modes. The modal parameters are evaluated from estimated complex mode residues ($\sigma_k \pm i\nu_k$) as $R_{1x,k}=2(\zeta_{x,k}\omega_{nx,k}\sigma_k-\omega_{dx,k}\nu_k)$, $R_{2,k}=2\sigma_k$. Similar terminology is used in the normal direction (Y). The use of transfer functions in frequency- and time-domain predictions of chatter vibrations can be found in Altintas et al. [9,15]. Using the identified cutting coefficients, the cutting forces are predicted for slot milling of Al7075 at different depths. The predicted and measured cutting forces agreed well, as can be seen from two sample test results shown in Fig. 7. The machine tool was unable to handle larger depth of cuts due to chatter and its limited torque capacity. The chatter stability lobes of the cutter are predicted using time-domain as well as frequency-domain analytical methods. The time-domain simulation considers the non-linearities in the process, such as varying cutting coefficients along the insert, discontinuities along the flute due to inserts, and tool jumping out of cut due to excessive vibrations. The frequency-domain analytical solution assumes constant average cutting coefficient and continuous cutting edges like in regular end mills. The stability lobes for half immersion down milling are predicted and experimentally verified with 0.050 mm/tooth feed rate (Fig. 8). The presence of chatter is monitored in the spectrum of sound signals measured using a microphone placed close to the cutting zone. Although the analytical chatter stability assumes a simplified, linear process model, it is still able to predict the chatter stability

Table 2
The transfer function parameters of Cutter I

Direction	Mode	ω_n (Hz)	ζ (%)	Mode residue (m/N) ($\sigma_k \pm i\nu_k$)
X	1	269.20	4.81	$(10.097-i8.760)\times10^{-6}$
	2	447.51	4.66	$(25.835-i105.161)\times10^{-6}$
	3	573.79	4.69	$(2.976-i57.900)\times10^{-6}$
	4	1837.50	2.94	$(54.251-i98.720)\times10^{-6}$
	5	2843.05	3.10	$(108.761-i29.515)\times10^{-6}$
	6	3065.05	1.13	$(63.293-i0.188)\times10^{-6}$
	7	4007.50	0.81	$(-8.380-i31.021)\times10^{-6}$
Y	1	495.47	3.32	$(8.428-i169.651)\times10^{-6}$
	2	1850.98	2.68	$(18.614-i76.902)\times10^{-6}$
	3	2115.10	1.67	$(16.382-i33.327)\times10^{-6}$
	4	3134.97	4.74	$(168.391-i191.999)\times10^{-6}$
	5	3991.89	0.91	$(5.962-i17.500)\times10^{-6}$

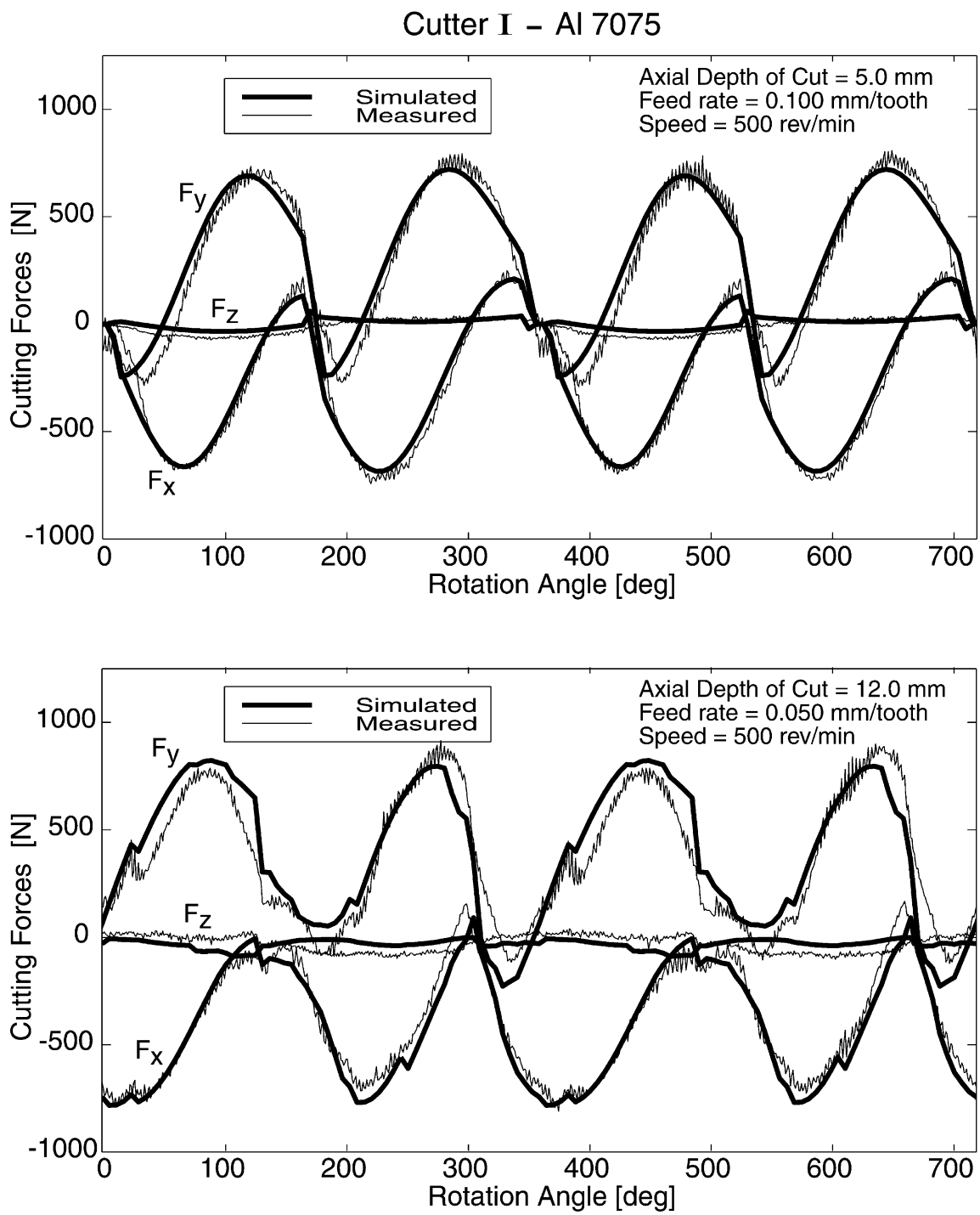

Fig. 7. Measured and predicted cutting forces for Al7075 with Cutter I. Cutting type is slotting. See Fig. 6 for tool geometry and Table 1 for cutting coefficients.

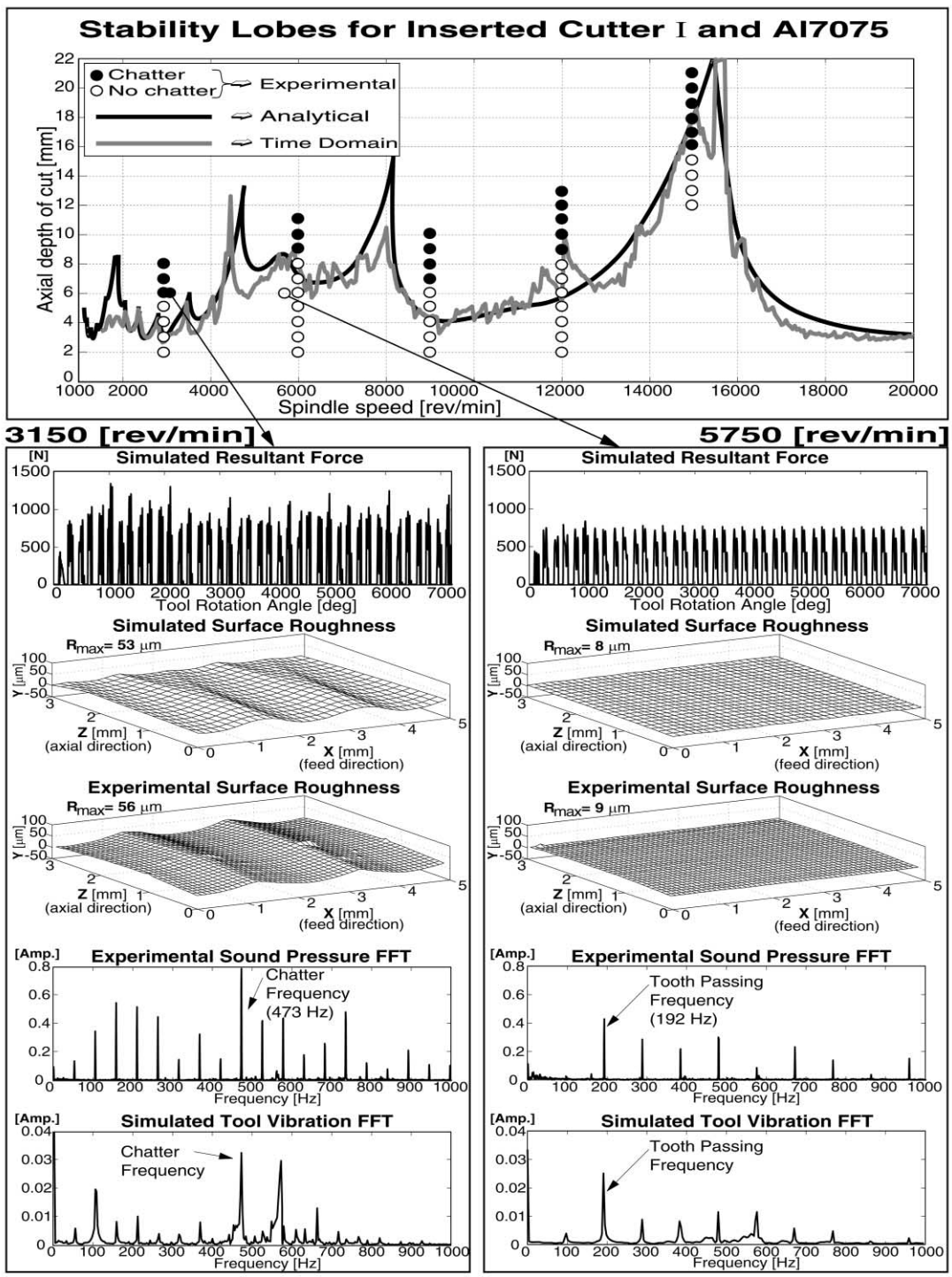

Fig. 8. Stability lobes for Al7075 with Cutter I (see Fig. 6). Cutting conditions: half immersion down milling, N_t=2 flutes, diameter=25.4 mm, feed rate=0.050 mm/tooth. See Table 1 for cutting coefficients of Al7075 and Table 2 for the transfer function parameters.

lobes quite satisfactorily. The stability lobe generation in the time domain took approximately two days of computer time and only few seconds in the frequency domain on a personal computer. The stability lobes indicated the presence of chatter at an axial depth of cut of 6.0 mm and spindle speed of 3150 rev/min. The measured and simulated values of surface finish and chatter vibration spectra are in good agreement. The chatter is caused by the first bending mode (473 Hz) of the spindle–cutter assembly. When the speed is increased to 5750 rev/min, the chatter disappeared as predicted by the stability lobe diagram and time-domain simulations.

4.2. Milling of Ti6Al4V with Cutter II

Titanium alloy Ti6Al4V is milled using a Mitsubishi LER1606W20 R98244 cutter with two flutes and two different rectangular inserts (Mitsubishi CCMX083508ENA and ZCMX083508ERA HTi20T). There are three inserts placed on each flute. The cutter design model is formed as (Fig. 9)

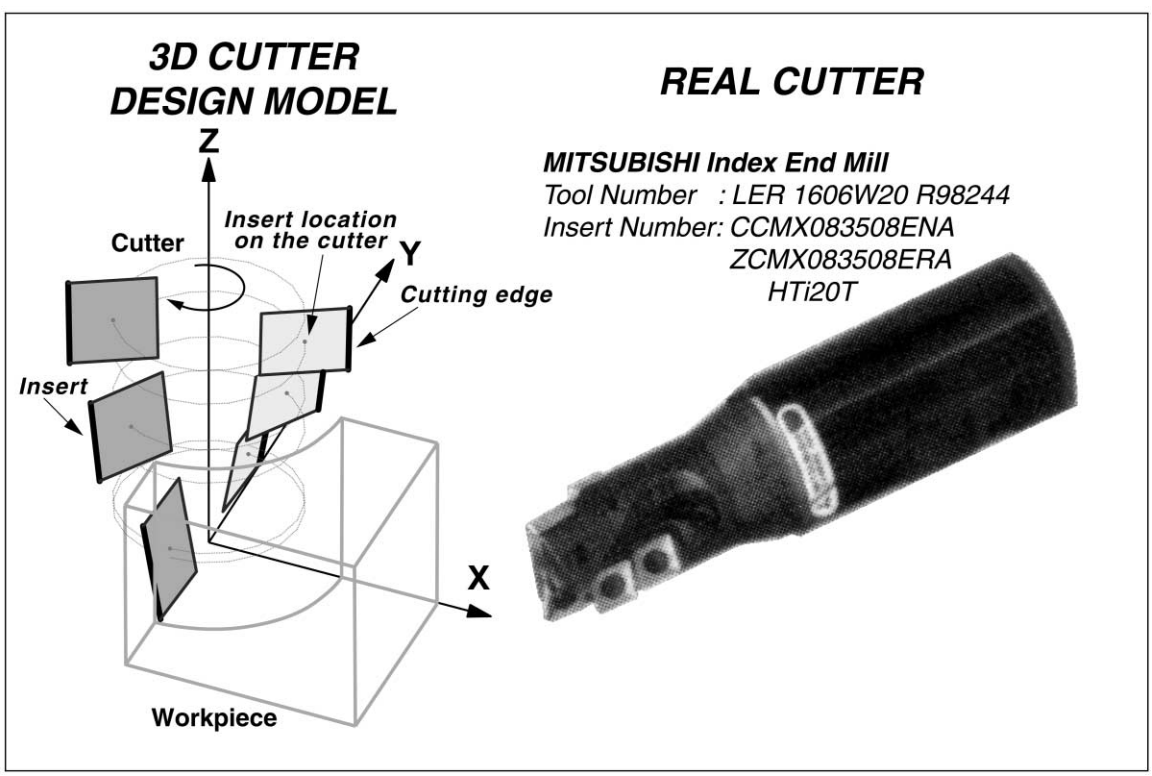

Fig. 9. Mitsubishi inserted cutter Cutter II (cutter number: LER1606W20 R98244; insert numbers: CCMX083508ENA, “insert dimensions *a*=8.0 mm, *b*=8.0 mm” and ZCMX083508ERA, “insert dimensions *a*=8.0 mm, *b*=10.0 mm”, HTi20T). See Eq. (10) for insert location parameters. Shank diameter=31.75 mm, cutter diameter=25.4 mm, two flutes, three inserts on every flute.

$$\boldsymbol{D}_{\mathrm{M}}=\begin{bmatrix} 3 & 3 & 3 & ; & 4 & 3 & 3 \\ 4.0 & 12.8 & 21.6 & ; & 5.0 & 16.5 & 25.3 \\ 8.7 & 8.7 & 8.7 & ; & 8.7 & 8.7 & 8.7 \\ 0.0 & 0.0 & 0.0 & ; & 0.0 & 0.0 & 0.0 \\ -10.0 & -10.0 & -10.0 & ; & -10.0 & -10.0 & -10.0 \\ 0.0 & 330.0 & 300.0 & ; & 180.0 & 150.0 & 120.0 \end{bmatrix}. \tag{10}$$

The first row indicates rectangular insert types 3 and 4. Both inserts have identical geometry except the cutting edge lengths. Insert 3 has edge dimensions a=8.0 mm and b=8.0 mm, and Insert 4 has a=8.0 mm and b=10.0 mm. Insert 4 is used as a wiper blade to smooth the cut surface. The cutting coefficients of the inserts are identified from slot milling tests conducted at different depths of cut (1.0–5.0 mm) and feed rates (0.020–0.080 mm/tooth), and given in Table 3. The insert edge geometry does not change beyond the first 5.0 mm length, thus the cutting coefficients remain the same as the values at z=5.0 mm. The spindle speed was 500 rev/min. The cutting coefficients change as a function of the insert's axial contact (z) with the material. The simulated and experimentally measured cutting forces for two sample cases are given in Fig. 10. The first case is slot milling with 5.0 mm axial depth of cut and 0.050 mm/tooth feed, and the second case is half immersion down milling with 16.0 mm axial depth of cut with 0.030 mm/tooth feed. The spindle speed was 500 rev/min. The measured and predicted cutting forces are in good agreement.

5. Conclusion

A generalized mathematical model for inserted cutters has been developed. The model allows placing different inserts on the cutter body mathematically. Each insert is placed on the cutter body by defining its center from a cutter body coordinate system. The inserts can be oriented by

Table 3
The cutting coefficients for Ti6Al4V with Cutter II ($0 \le z \le 5.0$ mm). Between 5.0 mm and 10.0 mm, the cutting coefficients are constant and the same as the values used at z=5.0 mm. The edge contact position (z) is expressed in millimeters

Cutting coefficient	Fitted curve	Correlation coefficient
K_{tc} (N/mm^2)	$81.8z^2-405.3z+2562.1$	0.8232
K_{rc} (N/mm^2)	$110.7z^2-511.1z+1862.3$	0.8931
K_{ac} (N/mm^2)	$-135.2z^2+935.8z-1697.9$	0.8803
K_{te} (N/mm)	$-4.83z^2+17.50z+25.80$	0.8260
K_{re} (N/mm)	$-5.84z^2+26.74z+86.4$	0.9563
K_{ae} (N/mm)	$-4.83z^2+35.81z-62.80$	0.9968

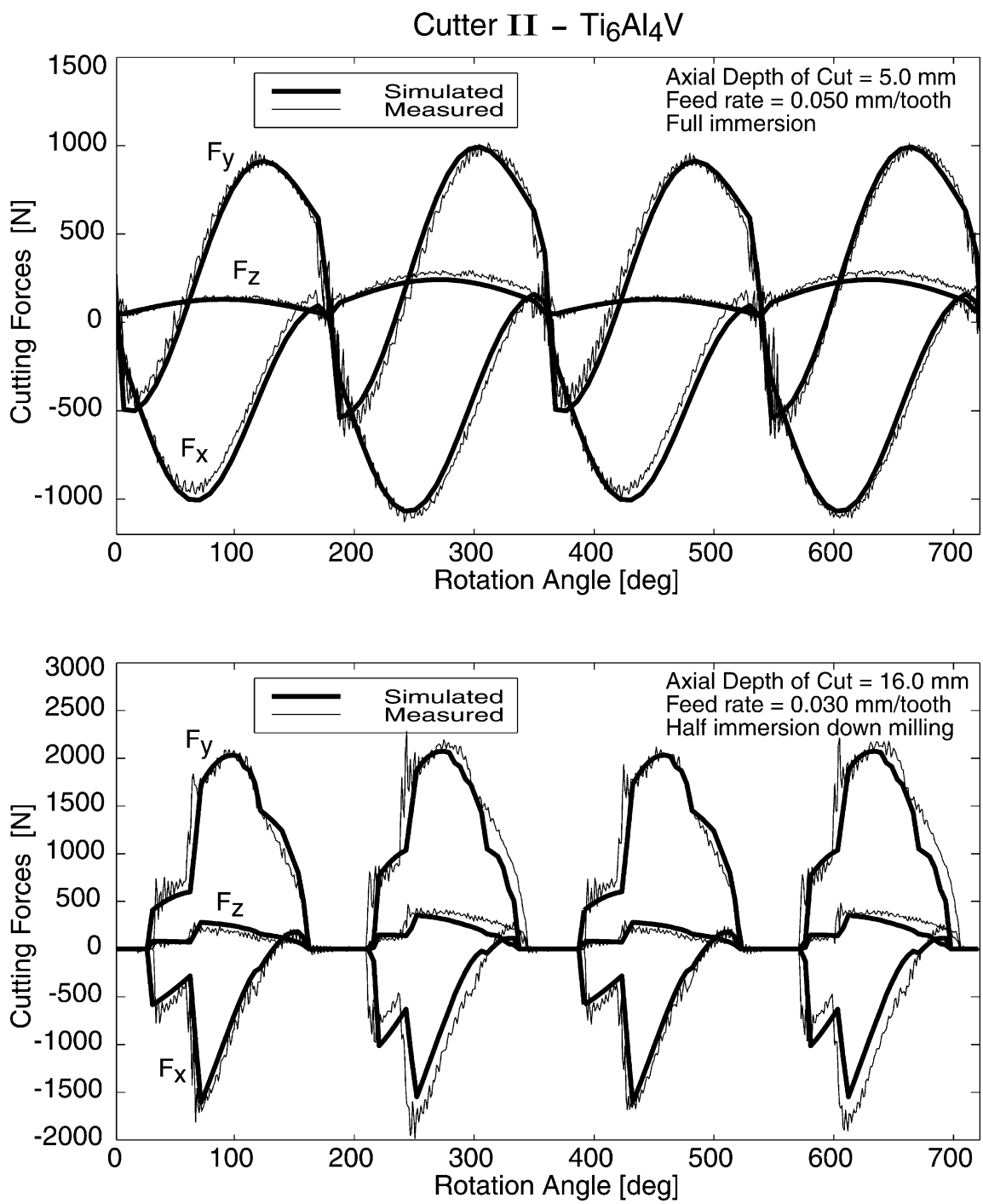

Fig. 10. Measured and predicted cutting forces for Ti6Al4V with Cutter II. Spindle speed is 500 rev/min. See Fig. 9 for tool geometry and Table 3 for cutting coefficients.

rotating them about the three axes of the cutter body. The insert geometry is defined individually in a local coordinate system by its edge dimensions and shapes. By combining the vectorial representation of the insert center and cutting edge, the cutting edge of each insert is defined. The chip thickness, cutting force, chatter vibrations, dimensional surface finish and stability lobes of the milling process generated by the arbitrarily inserted cutters are evaluated. The proposed model allows the analysis of general indexed cutters, and it is proven experimentally using two industrial indexed cutters in milling of Al7075 and Ti6Al4V alloys.

Acknowledgements

This research was supported by NSERC, General Motors, Pratt and Whitney Canada and Boeing under a Cooperative Research and Development Research Grant (NSERC 11R80193).

References

[1] R. Wertheim, A. Satran, A. Ber, Modifications of the cutting edge geometry and chip formation in milling, Annals of the CIRP 43 (1) (1994) 63–68.
[2] H.J. Fu, R.E. Devor, S.G. Kapoor, A mechanistic model for the prediction of the force system in face milling operation, ASME Journal of Engineering for Industry 106 (1) (1984) 81–88.
[3] H.S. Kim, K.F. Ehmann, A cutting force model for face milling operations, International Journal of Machine Tools and Manufacture 33 (5) (1993) 651–673.
[4] F. Gu, S.G. Kapoor, R.E. Devor, P. Bandyopadhyay, An enhanced cutting force model for face milling with variable cutter feed motion and complex workpiece geometry, Transactions of the ASME, Journal of Manufacturing Science and Engineering 119 (4) (1997) 467–475.
[5] A. Spence, Y. Altintas, A solid modeler based milling process simulation and planning system, Transactions of the ASME, Journal of Engineering for Industry 116 (1994) 61–69.
[6] W.J. Endres, R.E. DeVor, S.G. Kapoor, A dual-mechanism approach to the prediction of machining forces: Part I — Model development; Part II — Calibration and validation, Transactions of the ASME, Journal of Engineering for Industry 117 (1995) 526–541.
[7] S.A. Spiewak, Analytical modeling of cutting point trajectories in milling, Transactions of the ASME, Journal of Engineering for Industry 116 (1994) 440–448.
[8] E. Budak, Y. Altintas, E.J.A. Armarego, Prediction of milling force coefficients from orthogonal cutting data, Journal of Manufacturing Science and Engineering, Transactions of the ASME 118 (1996) 216–224.
[9] Y. Altintas, P. Lee, Mechanics and dynamics of ball end milling, Transactions of the ASME, Journal of Manufacturing Science and Engineering 120 (1998) 684–692.
[10] K.F. Ehmann, S.G. Kapoor, R.E. DeVor, I. Lazoglu, Machining process modeling: a review, Transactions of the ASME, Journal of Manufacturing Science and Engineering 119 (4B) (1997) 655–663.
[11] M.E. Martellotti, An analysis of the milling process. Part II: Down milling, Transactions of the ASME 67 (1945) 233–251.
[12] D. Montgomery, Y. Altintas, Mechanism of cutting force and surface generation in dynamic milling, Transactions of the ASME, Journal of Engineering for Industry 113 (1991) 160–168.
[13] S. Engin, Y. Altintas, Mechanics and dynamics of general milling cutters. Part I: helical end mills, International Journal of Machine Tools and Manufacture 41 (2001) 2195–2212.

[14] Y. Altintas, D. Montgomery, E. Budak, Dynamic peripheral milling of flexible structures, Transactions of the ASME, Journal of Engineering for Industry 114 (1992) 137–145.
[15] Y. Altintas, E. Budak, Analytical prediction of stability lobes in milling, Annals of the CIRP 44 (1) (1995) 357–362.
[16] CutPro, Analytic and time-domain process simulation software package — milling module [online], Available at http://www.malinc.com/CutPro/index.htm, University of British Columbia, Manufacturing Automation Laboratory, 2000.